Cislunar end-of-life strategies based on an aware usage of key dynamical objects

Mathilda Bolis(1), Elisa Maria Alessi(2), Joan Pau Sánchez Cuartielles (3), Camilla Colombo (1), Stéphanie Lizy-Destrez (3)

(1) Dipartimento di Scienze e Tecnologie Aerospaziali (DAER), Politecnico di Milano
Milano, Italy
Email: mathilda.bolis@polimi.it, camilla.colombo@polimi.it

(2) Istituto di Matematica Applicata e Tecnologie Informatiche "Enrico Magenes", Consiglio Nazionale delle Ricerche (IMATI-CNR)
Milano, Italy
Email: elisamaria.alessi@cnr.it

(2) Institut Supérieur de l'Aéronautique et de l'Espace (ISAE-SUPAERO)
Toulouse, France
Email: joan-pau.sanchez@isae-supaero.fr, stephanie.lizy-destrez@isae-supaero.fr

***Abstract* – As space traffic in the Earth's vicinity continues to grow rapidly, cislunar space is emerging as the next frontier of space exploration. To support its sustainable utilisation, the development of robust and cost-effective End-of-Life (EoL) disposal strategies is of primary importance. In this work, unstable manifold trajectories generated from two Halo orbits, one at L_1 and one at L_2 of the Earth-Moon (EM) system, are propagated within the coupled Circular Restricted Three Body Problem (CR3BP) framework. Maps describing the outcomes of disposal trajectories as a function of the phase angle and the relative phase between the EM and Sun-Earth (SE) systems at manifold insertion are presented for the cases under analysis. Finally, a subset of these trajectories is identified as viable disposal options and further refined accordingly, providing estimates of the Zero Velocity Curves (ZVCs) closure cost for heliocentric disposal options, as well as impact locations, velocities, and angles for lunar impacts and Earth re-entries.**

I. INTRODUCTION

An exponential increase in space traffic within the cislunar region is expected in the coming years, given the growing number of missions targeting this strategic region of space, either to exploit lunar resources or to establish an outpost for future human exploration. Alongside the technological developments required to support this, significant attention is being given to limit the generation of a space debris problem in the region. Indeed, a key priority is to establish a robust space situational awareness infrastructure in this area, characterised by strong non-linear dynamics and subject to the combined gravitational influence of the Earth and Moon. The aim is to prevent fragmentation events and collisions involving operational and non-operational objects, which has led to a recent increase in studies focusing on these aspects, e.g. [1][2][3][4].

A fundamental prerequisite for achieving this objective is the development of robust and low-cost End-of-Life (EoL) disposal strategies, facilitating the integration of satellite decommissioning into lunar mission design, thereby mitigating the risk of debris generation. Disposal at EoL has been extensively studied for missions operating in the vicinity of the Earth, as well as for some missions operating at the Sun-Earth (SE) system's Lagrangian points, e.g. [5]. For what concerns cislunar space, studies about disposal design focused mainly on the Near Rectilinear Halo Orbit (NRHO) reference for the Lunar Gateway, e.g. [3]. However, a comprehensive framework for investigating disposal in cislunar space remains an open area of research.

According to ESA [6], within cislunar space four main disposal strategies can be applied: heliocentric disposal, controlled lunar impact, Earth re-entry and graveyard orbit insertion. Given a mission, the most appropriate strategy should be selected based on the characteristics of the satellite's operational orbit, the ΔV budget, the time available for disposal, and the level of safety required by regulations for current and future operations.

This work presents an analysis of the evolution of unstable manifolds, assumed as the dynamical backbone of disposal trajectories, associated with two Halo orbits in the Earth–Moon (EM) system, one centred at EM-L_2 and one at EM-L_1, as the Halo family is considered of particular relevance for future mission architectures. Unstable manifolds are propagated thanks to an approximation of real cislunar dynamics, the coupled Circular Restricted Three Body Problem (CR3BP), accounting for the influence of the Earth, the Moon and the Sun in the system. First, the evolution of the outcomes of the disposal trajectories is shown as a function of the phase angle along the reference periodic orbit from which the manifold departs, θ_0, and the relative phase between the EM and SE systems at the unstable manifold insertion, α_0. Then, as disposal trajectories' evolution can result in either escape towards the SE-L_1 or SE-L_2, impact with the Moon, impact with the Earth, escape from the EM system but not from the SE one, or no escape from the EM system, some of the trajectories obtained are associated with the preliminary design of a certain type of disposals, i.e. heliocentric disposal, lunar impact or Earth re-entry. It is consequently shown how it is possible to improve the disposal design for such cases by selecting the scenarios that best comply with existing space sustainability guidelines; assessing the Zero Velocity Curves (ZVCs) closure cost in the case of heliocentric disposal and by identifying impact locations, velocities and angles in the case of lunar impacts and Earth re-entries. The main objective of this work is to outline a preliminary framework for disposal design of spacecraft operating on periodic orbits in the EM system, focusing on the influence of the Sun on disposal trajectories and assessing the feasibility of the proposed scenarios.

II. DYNAMICAL FRAMEWORK

The dynamical model used in the analysis is the EM and SE coupled CR3BP. The CR3BP has traditionally been used to approximately describe the motion of an object with negligible mass in a region of space strongly influenced by the gravitational attraction of two major bodies, which are assumed moving in circular orbits around their common Centre of Mass (CoM) [7]. In the case of the coupled CR3BP, the two main bodies involved are either the Earth and the Moon, or the Sun and the Earth, depending on which between the Moon or the Sun has a stronger influence on the trajectory. As in the classical CR3BP formulation, the state of an object is defined in a non-dimensional, rotating coordinate system, having its origin at the primaries CoM and them lying along the x-axis, with the positive direction pointing towards the smaller primary, and the z-axis is orthogonal to the plane of the two major bodies motion. The dimensionless gravitational constant of the EM system is fixed equal to 0.01215, that of the SE system to 3.0404×10^{-6}. Lengths are scaled relative to the average EM or SE distances, fixed as 384399 km and 149597870.7 km respectively, and times such that the average angular velocity of the rotating frames equals 1. Thus, length units are expressed as either LU_{EM} or LU_{SE}, and time units as either TU_{EM} or TU_{SE}. Within the CR3BP, only one integral of motion exists, termed the Jacobi Constant (JC), which can be associated with an energy like constant E, such that $E = -JC/2$.

Five equilibrium points, known as the Libration or Lagrange points L_1 to L_5, can be identified and the regions of admissible motion for a particle are characterised based on its energy: for a given value of the JC, the motion is constrained to a five dimensional energy surface embedded in a six dimensional phase space. The boundaries of the corresponding regions of motion, known as Zero Velocity Curves (ZVCs), are defined as the loci where the velocity of the particle is zero. The two CR3BP models are approximated as coplanar and are linked via a coordinate change and the evolution of their relative phase over time, as outlined in [8]. Let us define the phase of the EM system relative to the SE system as $\alpha(t)$, shown in Fig. 1.

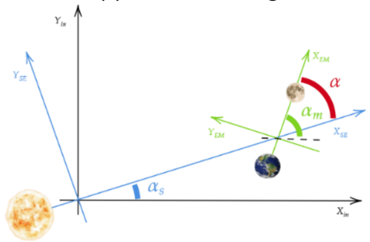

Fig. 1. Schematic representation of the approximation considered to model the relationship between the SE and the EM rotating frames.

The angle $\alpha(t)$ is used to determine the geometric relationship between the two systems at any time, with its evolution given by:

$$\alpha(t) = \alpha_0 + \frac{\omega_{EM}-\omega_{SE}}{\omega_{EM}} t_{EM} \qquad (1)$$

being ω_{EM} and ω_{SE} the non-dimensional angular velocities of the two rotating frames, fixed as 2.6653×10^{-6} and 1.9909×10^{-7} respectively, t_{EM} the propagation time in the EM system, and α_0 the initial relative phase between the two models. A trajectory leaving a periodic orbit of the EM system is propagated considering only the EM CR3BP until the influence exerted by the Moon on the spacecraft is less than that exerted by the Sun. At this point, the dynamical model switches to the SE CR3BP. The dynamics are modelled as switching between the EM and SE CR3BP as many times as necessary, considering at each timestep only either the EM or the SE CR3BP. The coupled CR3BP shares similarities with the Bicircular Restricted Four Body Problem, e.g. [3], while retaining the assumptions and fundamental quantities of the classical CR3BP. Moreover, it allows for potential extensions of the model, including the inclusion of the Moon's inclination with respect to the ecliptic into the dynamical framework. As a final remark, the coupled CR3BP is an autonomous dynamical model, since its equations of motion are time-independent. However, the coordinate transformation from the EM to the SE frame, and vice versa, depends on $\alpha(t)$ and it is therefore non-autonomous.

III. REFERENCE PERIODIC ORBITS DEFINITION AND SIMULATION SET UP

The reference periodic orbits considered in the simulation are two Halos, one centred at EM-L_1 and one at EM-L_2. Given an initial guess, periodic orbits are defined thanks to a differential correction algorithm enforcing periodicity, orthogonality and symmetry with respect to a certain reference plane [9]. Numerous families of periodic orbits can be defined in a three-body system [10], with Halo orbits constituting just one class, among the most important for future mission applications. The selected reference Halo orbit in EM-L_2 is characterised by $JC = 3.0988$, $SI = 209.8644$ and $r_p = 42860.49$ km, where SI is the linear stability index, indicating an unstable orbit when greater than 1, and r_p the perilune radius. The Halo orbit in EM-L_1 is characterised by $JC = 3.0986$, $SI = 264.4997$ and $r_p = 44551.84$ km. These two orbits have been selected for the present analysis as representative examples of the behaviour of disposal trajectories associated with Halo orbits in the EM system. They are also characterised by similar initial energy levels and stability properties, to facilitate a preliminary comparison between the dynamical behaviours of orbits centred at EM-L_1 and L_2.

Disposal trajectories are computed by initially inserting the spacecraft onto the unstable manifolds of the periodic orbits. The unstable manifold direction is regarded as the most effective for disposal, as it corresponds to the direction of the motion that asymptotically diverges from the reference orbit. The nondimensional perturbation used to insert the spacecraft into the unstable manifold is fixed at 10^{-4}, which could be considered as an initial disposal manoeuvre in the order of about 10^{-3} m/s. Note that a variation in the initial perturbation, or ΔV, corresponds to a rotation of the manifold along θ_0. The direction of the unstable manifold is computed as from classical dynamical systems theory, as discussed for example in [11]. As shown in Fig. 2 and Fig. 3, for each periodic orbit, two manifold branches exist: one directed towards the L_1 or L_2 bottlenecks of the EM system (blue), and the other directed towards the Moon (red).

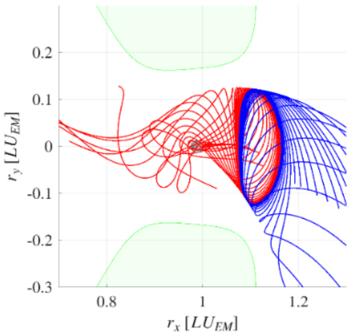

Fig. 2. Unstable manifold trajectories from the reference Halo orbit in EM-L_2, propagated for 1 month. Blue: branch escaping the lunar vicinity (E_2); red: branch directed toward the Moon (M_2). In green: ZVCs of the EM system evaluated at the JC of the reference orbit.

Both unstable manifold branches are taken into account in the identification of possible disposal scenarios, as will be further detailed in the following sections. From this point onward, the branch of the manifold associated with the L_1 reference Halo orbit that initially evolves toward EM-L_1 will be denoted as E_1, while the branch directed toward the Moon will be denoted as M_1.

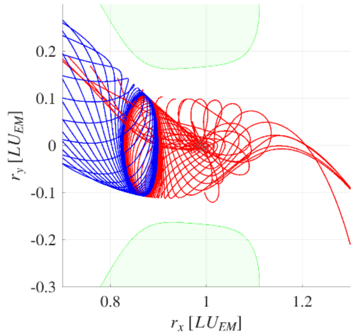

Fig. 3. Unstable manifold trajectories from the reference Halo orbit in EM-L_1, propagated for 1 month. Blue: branch escaping the lunar vicinity (E_1); red: branch directed toward the Moon (M_1). In green: ZVCs of the EM system evaluated at the JC of the reference orbit.

Similarly, for the L_2 reference Halo orbit, the branch initially evolving toward EM-L_2 will be referred to as E_2, and the one directed toward the Moon as M_2. Manifold trajectories are discretised as a function of the periodic orbit phase angle at departure, θ_0, which is a parametrisation of the periodic orbit period in the EM-CR3BP and is considered equal to 0° at apolune and to 180° at perilune. Simulations are performed by progressively varying the values of θ_0 and α_0, the phase of the EM system with respect to the SE system at periodic orbit departure, see Eq. (1), using a discretisation step of 2° for each parameter. The propagation is carried out with the ode113 MATLAB built-in integrator, for a maximum propagation time of 12 months. Each trajectory on the unstable manifold is propagated in the coupled CR3BP, and the possible outcomes are: a) escape through SE-L_2; b) escape through SE-L_1; c) impact with the Moon; d) impact with the Earth, with propagation stopped at an altitude of 150 km; e) no escape through either the SE-L_1 or the SE-L_2 bottleneck and no impact; or f) no escape through the EM-L_2 bottleneck and no impact.

IV. EVOLUTION OF DISPOSAL TRAJECTORIES BEHAVIOURS AS A FUNCTION OF θ_0 AND α_0

As introduced in the previous section, the first step in the analysis is to develop maps that identify trajectories behaviours as the parameters θ_0 and α_0 vary. An example of such maps is shown in Fig. 4 for the E_2 manifold branch, related with the reference Halo orbit in L_2. The map shows the propagation outcome in colour, with green identifying conditions where the manifold trajectory escapes from SE-L_2; blue, conditions where the manifold trajectory escapes from SE-L_1; purple, Moon impacts; red, Earth re-entries; yellow, conditions where there is neither escape from the SE ZVCs nor impact; and white, conditions where there is neither escape from the EM ZVCs nor impact. From a dynamical perspective, the behaviour exhibited by these kind of maps is of particular interest. Just to cite some

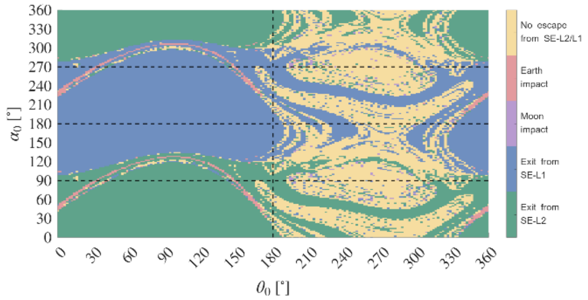

Fig. 4. Map showing the evolution of the unstable manifold propagation outcome as a function of θ_0 and α_0. Reference Halo orbit in L_2, branch E_2 (blue in Fig. 2).

examples, it is interesting to observe the symmetry in the solution space with respect to α_0 = 180°, and it can be demonstrated that the values of θ_0 leading to trajectories prone to escape correspond to cases exhibiting hyperbolicity with respect to the Earth early on. A detailed analysis of these aspects will be presented in a future work; here, the focus is instead placed on the robustness and practical feasibility of possible disposal strategies. Indeed, maps such as the one shown in Fig. 4 can be used to identify natural paths to eventual disposal scenarios, which can be targeted just by knowing the combination of α_0 and θ_0, i.e. initial conditions, that leads to them. The map relative to M_2, related with the reference Halo orbit in L_2, is presented in Fig. 5

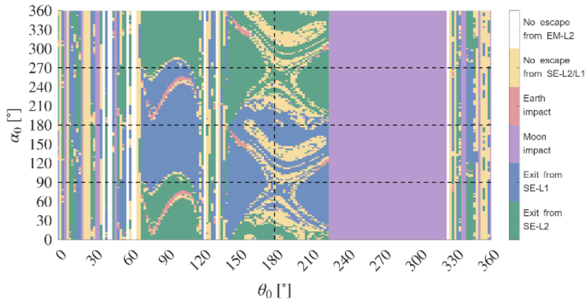

Fig. 5. Map showing the evolution of the unstable manifold propagation outcome as a function of θ_0 and α_0. Reference Halo orbit in L_2, branch M_2 (red in Fig. 2).

Since the objective is to identify conditions that lead to safe and robust disposal scenarios, it is possible to note the following just by observing the maps:

- Heliocentric disposal would be ideal if performed at the centre of the escape isles which can be found for $\theta_0 \in [0°, 180°]$, in the map relative to E_2 (Fig. 4).
- Lunar impacts would be the safest if performed for $\theta_0 \in [225°, 320°]$, M_2 (Fig. 5).
- No consistent regions leading to Earth re-entry are observed in the maps. Nonetheless, selected conditions may deserve further analysis for both manifold branches, especially those associated with the parabola-like structures found at the boundaries of the escape isles, for example, in Fig. 4 for $\theta_0 \in [0°, 180°]$.

Conditions leading, for instance, to heliocentric trajectories or lunar impacts can also be found in other regions of the maps; however, they are not discussed here in detail, as the aim is to provide a general overview of the conditions enabling the best and ideally most robust disposal scenarios.
Fig. 6 and Fig. 7 show the maps relative to the unstable manifold behaviour for the reference Halo orbit in L_1, E_1 and M_1 respectively.

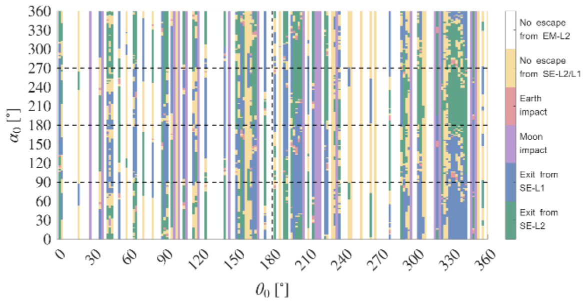

Fig. 6. Map showing the evolution of the unstable manifold propagation outcome as a function of θ_0 and α_0. Reference Halo orbit in L_1, branch E_1 (blue in Fig. 3).

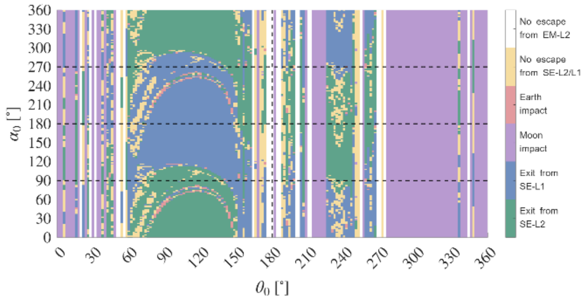

Fig. 7. Map showing the evolution of the unstable manifold propagation outcome as a function of θ_0 and α_0. Reference Halo orbit in L_1, branch M_1 (red in Fig. 3).

As done for the Halo orbit in L_2, it is consequently possible to conclude that:

- The natural path followed by branch E_1 (Fig. 6) is highly scattered, being governed by strongly non-linear dynamics, and it is therefore not well suited for disposal applications without the inclusion of additional manoeuvres.
- Heliocentric disposal is best fitted for the escape isles that can be found in Fig. 7, branch M_1, for $\theta_0 \in [60°, 150°]$
- Lunar impact would be the best if applied for $\theta_0 \in [270°, 330°]$, considering M_1 (Fig. 7).
- As for the reference L_2 Halo consistent regions leading to Earth re-entries are not found, but the conditions leading to the parabola-like shape for $\theta_0 \in [60°, 150°]$ in Fig. 7 may still be interesting to analyse.

Having identified the regions in the maps associated with the most suitable disposal scenarios for both the orbits considered, further analyses are conducted to assess their practical implementation.

V. HELIOCENTRIC DISPOSAL

When targeting heliocentric disposal, the ideal scenario would involve direct escape, i.e. trajectories that escape the EM system and then the SE system quickly and easily without leading to multiple revolutions around the Moon or the Earth before passing through one of the SE ZVCs bottlenecks. Examples of direct escape trajectories departing from the reference Halo in L_1 (M_1, green) and L_2 (E_2, pink) are reported in the SE rotating frame in Fig. 8.

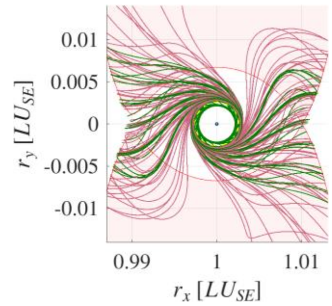

Fig. 8. Direct escape trajectories departing from the reference Halo orbit in L_1 (green) and L_2 (pink). Moon's orbit is represented by the dashed yellow line, the red area represents the SE system ZVCs evaluated at SE-L_2.

If direct escape cannot be achieved, indirect escape remains an option for heliocentric disposal, but it would lead to longer disposal phases and increased operational efforts and risks. The conditions for direct escape as a function of θ_0 and α_0 for the L_2 reference Halo orbit, branch E_2, are shown in Fig. 9.

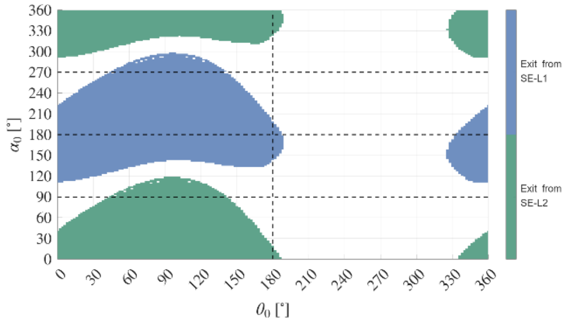

Fig. 9. Map of direct escape conditions as a function of θ_0 and α_0. Reference Halo orbit in L_2, branch E_2 (blue in Fig. 2).

These conditions reveal well-defined regions or "islands" in the maps, identifying solutions that enable direct escape in a safe and robust manner, especially when chosen near their centres. Also, it is important to mention that, from a sustainability perspective, escape via SE-L_2 is generally preferable to escape via SE–L_1 but, nevertheless, scenarios involving SE-L_1 escape are included in the analysis for completeness.

As a second step in heliocentric disposal design, it is also necessary to close the ZVCs of the SE system once the spacecraft has escaped the Earth's vicinity, in order to prevent re-entry. In this work the magnitude of the manoeuvre needed to close the SE ZVCs is computed with an energetic approach, as described in [11], considering only the case in which the ZVCs closure manoeuvre is applied parallel to the local spacecraft velocity along the trajectory, but in the opposite direction.

Conditions and Times of Flight (ToFs) leading to a 10 m/s and 50 m/s ZVCs closure manoeuvre, considering all the possible escape option for the reference L_2 Halo, branch E_2, are reported in Fig. 10 and Fig. 11 respectively.

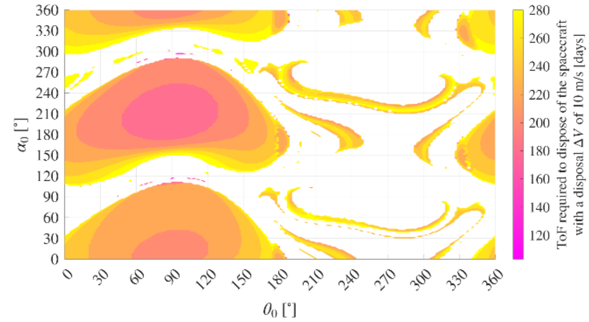

Fig. 10. Map showing the ToF required to achieve the ZVCs closure manoeuvre with a ΔV of 10 m/s, as a function of θ_0 and α_0. Halo orbit in L_2, branch E_2 (blue in Fig. 2).

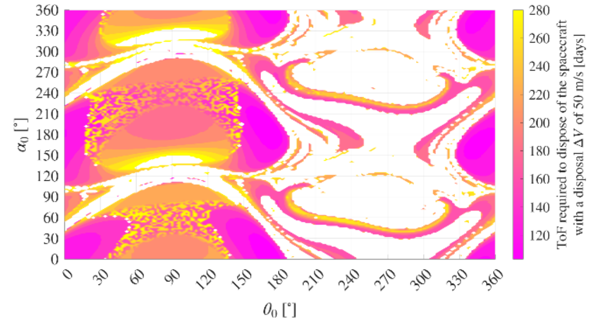

Fig. 11. Map showing the ToF required to achieve the ZVCs closure manoeuvre with a ΔV of 50 m/s, as a function of θ_0 and α_0. Halo orbit in L_2, branch E_2 (blue in Fig. 2).

ΔV values equal to 10 m/s and 50 m/s are considered as representative measures to assess how the ZVCs closure cost varies across the search space. By superimposing the map showing conditions leading to direct escapes with the ones describing the evolution of the ToF for the two possible ZVCs closure scenarios, it is possible to identify areas that lead to a fast, direct escape and a low-cost ZVCs closure. To achieve escape through L_2, assuming a $\Delta V = 50$ m/s for the ZVCs closure manoeuvre, the fastest solutions (with a ToF of approximately 4 months) are obtained at the boundaries of the direct escape regions, for $\theta_0 \in [0°, 30°]$ or $\theta_0 \in [150°, 180°]$, and $\alpha_0 \in [0°, 30°]$ or $\alpha_0 \in [300° \; 360°]$. If longer ToFs are acceptable, targeting the central regions of the direct escape "islands" yields more favourable solutions, with $\Delta V = 10$ m/s and a ToF of about 6 months. Note that, a clear drawback of heliocentric disposal is the relatively long waiting time before performing the ZVCs closure manoeuvre. However, larger injection maneuvers, with respect to the one considered, would tend to reduce the ToF. Indeed, this work demonstrates the feasibility of the proposed scenario, while future studies will investigate these aspects. In Fig. 12, the map identifying direct escapes related to the reference L_1 Halo orbit, branch M_1, is shown.

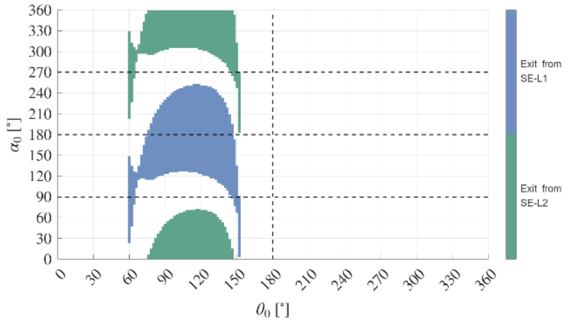

Fig. 12. Map of direct escape conditions as a function of as a function of θ_0 and α_0. Reference Halo orbit in L_1, branch M_1 (red in Fig. 3).

Fig. 13 and Fig. 14 report the evolution of the ToF to achieve a 10 m/s and 50 m/s ZVCs closure maneuver respectively.

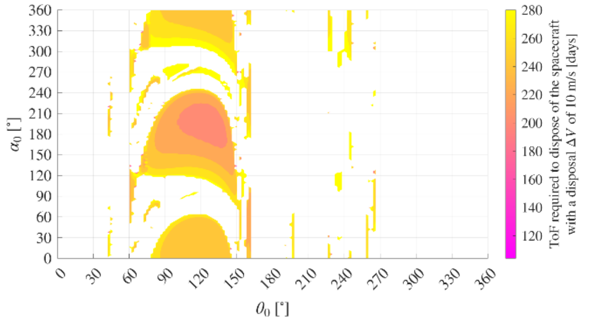

Fig. 13. Map showing the ToF required to achieve the ZVCs closure manoeuvre with a ΔV of 10 m/s, as a function of θ_0 and α_0. Halo orbit in L_1, branch M_1 (red in Fig. 3).

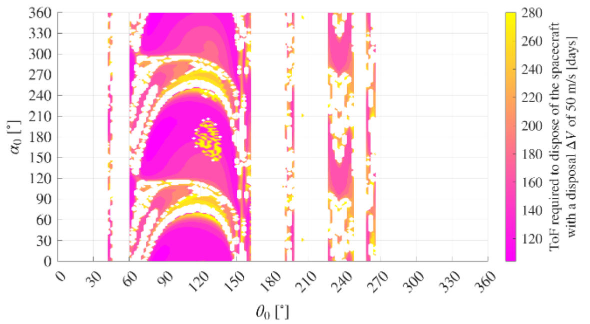

Fig. 14. Map showing the ToF required to achieve the ZVCs closure manoeuvre with a ΔV of 50 m/s, as a function of θ_0 and α_0. Halo orbit in L_1, branch M_1 (red in Fig. 3).

As a general rule, the same considerations derived for the reference L_2 Halo orbit can also be applied to the L_1 Halo, with an appropriate shift in the ranges of α_0 and θ_0 leading to a feasible heliocentric disposal scenario. Also the ToFs leading to heliocentric disposal are similar for both reference orbits considered.

VI. LUNAR IMPACT DISPOSAL

As for lunar impact disposal, the best conditions to obtain it following the manifold natural dynamic are defined as in section IV: $\theta_0 \in [225°, 320°]$ for the reference L_2 Halo, branch M_2, and $\theta_0 \in [270°, 330°]$ for the reference L_1 Halo, branch M_1. Note that these are the regions that lead to a lunar impact before escaping through EM-L_2. Trajectories leading to lunar impact after escape through EM-L_2, and thus influenced by the Sun, exhibit highly chaotic and hard to predict behavior. These are also isolated solutions in regions of no-escape behaviour (as happens in the map in Fig. 4) and are therefore not considered viable disposal options. Possible lunar impact disposal trajectories are shown in Fig. 15 in the EM rotating reference frame, green when departing from EM-L_1, branch M_1, and light-pink from EM-L_2, branch M_2.

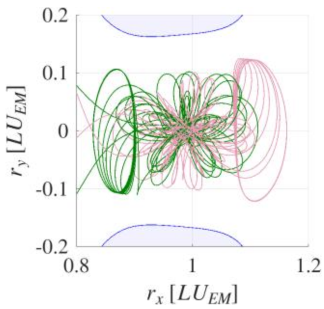

Fig. 15. Lunar impact trajectories departing from the reference Halo orbit in L_1 (green) and L_2 (light-pink). The blue area represents the EM system ZVCs evaluated at the JC of the initial reference orbit.

Impact locations, velocities and angles are computed thanks to impact states in the body-fixed Mean-Earth (ME) reference frame. To obtain the impact states in the ME reference frame, conditions in the EM rotating reference frame are first transformed in the Moon centred J2000 reference frame, with a procedure similar to the one described in [12]. Then, impact states in the Moon centred J2000 reference frame are rotated in the ME frame thanks to the *cspice_sxform* SPICE routine. Impact velocities are computed directly in the ME reference frame, while the impact angle, ϕ, is defined as the angle between the local tangent to the surface and the impact direction. Note that these transformations require the definition of the ephemeris time at impact, which is obtained as the sum of the initial ephemeris time and the ToF leading to impact. The initial ephemeris time is selected within the interval from 30th January 2029, 08:00, to 28th February 2029, 21:00, and is associated with the value of α_0 leading to a given impact trajectory. Impact locations, velocities and angles obtained for the reference Halo orbit in L_2, branch

M₂, are reported in Fig. 16.

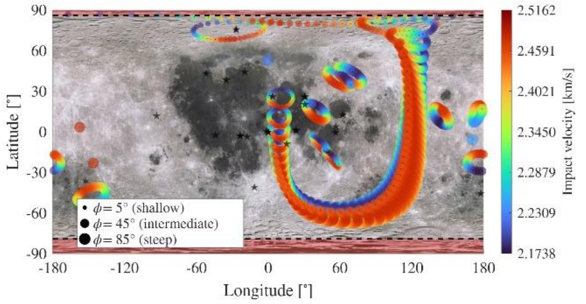

Fig. 16. Lunar impacts, displayed as a function of longitude and latitude. The color represent the impact velocity, while point size indicates the impact angle. Stars mark historical landing sites, and red regions highlight protected polar areas. Reference Halo orbit in L₂, branch M₂ (red in Fig. 3).

Impact velocities and angles are coherent with the ones found in previous studies, e.g. [2]. To provide a comprehensive framework of lunar impacts behaviour, the evolution of latitude and longitude as a function of θ_0 and α_0 is reported in Fig. 17 and Fig. 18 respectively.

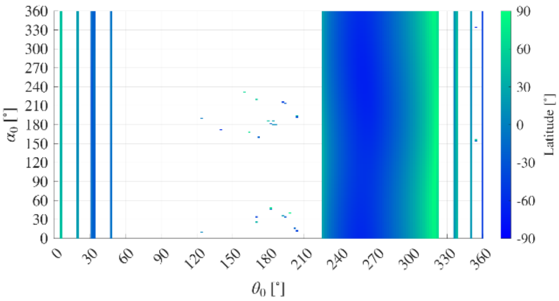

Fig. 17. Map of the evolution of the latitude reached by lunar impacts as a function of θ_0 and α_0. Reference Halo orbit in L₂, M₂ (red in Fig. 3).

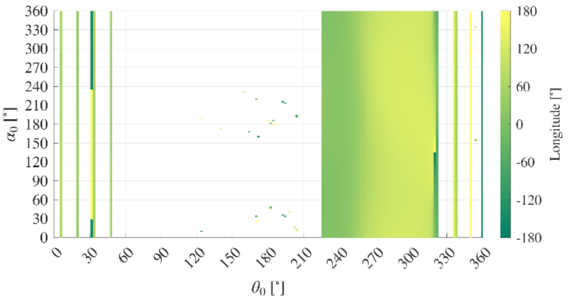

Fig. 18. Map of the evolution of the latitude reached by lunar impacts as a function of θ_0 and α_0. Reference Halo orbit in L₂, M₂ (red in Fig. 3).

By combining the information from Fig. 16, Fig. 17 and Fig. 18, it can be observed that longitude and latitude remain constant with α_0 and vary with θ_0. Accordingly, for a fixed θ_0, impact points form circular patterns, visible in Fig. 16, as α_0 varies. Also, α_0 (or the initial ephemeris time) mainly affects the impact velocity, whereas θ_0 influences the impact angle and location. From a space sustainability perspective, lower impact velocities reduce crater dimensions and the generation of eventual ejecta. These should so be targeted selecting the appropriate α_0. To avoid protected regions, it is necessary to remain distant from the lunar poles and ensure that impact trajectories do not intersect historical heritage sites. Considering these constraints, the most suitable region for lunar impacts corresponds in this case to departure conditions with $\theta_0 \in [270°, 300°]$. ToFs leading to these solutions are equal to about 19 days.
Impact locations, velocities and angles are reported in Fig. 19 for the reference L₁ Halo, M₁ branch.

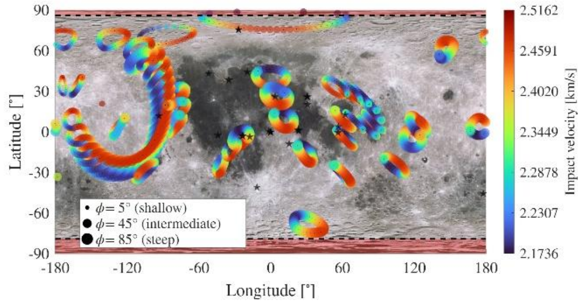

Fig. 19. Lunar impacts on the Moon's surface, displayed as a function of longitude and latitude. The color represent the impact velocity, while point size indicates the impact angle. Stars mark historical landing sites, and red regions highlight protected polar areas. Reference Halo orbit in L₁, branch M₁ (red in Fig. 3).

The evolution of latitude and longitude as a function of θ_0 and α_0 is similar to that obtained for the reference Halo orbit in L₂, as well as that of impact velocities and angles. The ideal option to obtain lunar impact in this case would be to target departure from $\theta_0 \in [290°, 320°]$, with the mean ToF required to impact the Moon in this range equal to about 16 days.

VII. EARTH RE-ENTRIES

As stated previously in section IV, no consistent regions leading to Earth re-entry are observed in the maps. Anyway, to give an idea of the behaviour of Earth re-entry trajectories, some examples are reported in Fig. 20.

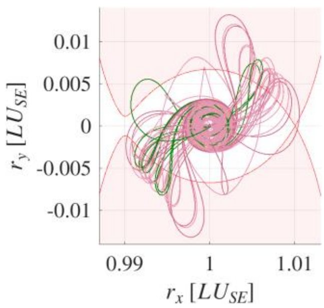

Fig. 20. Earth re-entry trajectories departing from the reference Halo orbit in L₁ (green) and L₂ (light-pink for branch M₂ and pink for branch E₂). Moon's orbit is represented by the dashed yellow line, the red area represents the SE system ZVCs evaluated at SE-L₂.

One of the most interesting observations is that many of the identified Earth re-entries exhibit profiles similar to

Weak Stability Boundary (WSB) transfers from Earth to Libration point orbits in the EM system. Earth re-entries can be classified into two subcategories: the first includes trajectories that impact the Earth and are primarily governed by the EM dynamics, even if part of their propagation occurs within the SE CR3BP; the second governed by the gravitational influence of the Sun, resembling reverse WSB transfers.

Impact locations, velocities, and angles are, in this case, computed in the Earth-Centered Earth-Fixed (ECEF) frame, following a procedure similar to that adopted for lunar impacts to transform states expressed in the EM rotating reference frame in the ME body-fixed frame. The results obtained relative to the reference Halo orbit in L_2, branch E_2 are reported in Fig. 21.

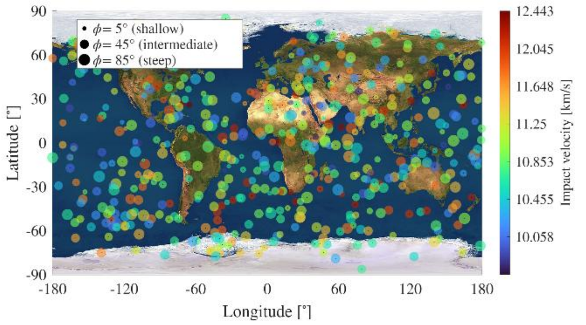

Fig. 21. Earth re-entry conditions, computed at 150 km from the Earth surface, displayed as a function of longitude and latitude. The color represent the impact velocity, while point size indicates the impact angle. Reference Halo orbit in L_2, branch E_2 (blue in Fig. 3).

Earth re-entry trajectories exhibit ToFs of 3-5 months and highly scattered impact locations, making it difficult to define clear disposal guidelines, in agreement with previous studies [2]. This indicates that Earth re-entry disposal cannot rely solely on the natural Sun-Earth-Moon dynamics and would likely require additional maneuvers. Results for the M_2 branch and the L_1 Halo are not reported, as they closely resemble those obtained for E_2.

VIII. CONCLUSIONS AND FUTURE WORKS

In this work, the dynamics of unstable manifolds departing from reference Halo orbits at L_1 and L_2 of the EM system have been analysed and, where possible, associated with potential disposal scenarios. Heliocentric disposal trajectories achieving direct escape have been identified, and the corresponding ZVCs closure costs have been evaluated. Additionally, lunar and Earth impact locations, velocities, and angles have been characterised. The objective of this study is to provide a preliminary overview of possible disposal strategies related to two reference Halo orbits in the EM system, one at L_1 and one at L_2, and to compare them.

IX. ACKNOWLEDGEMENTS

This research has received funding as part of the work developed for the agreement n. 2023-37-HH.0 for the project “Attività tecnico-scientifiche di supporto a CSSA/ISOC e simulazione di architetture di sensori per SST”, established between ASI, Italian Space Agency, and POLIMI, Politecnico di Milano.

X. REFERENCES

[1] D. Andrievskaia, I. Cáceres Ballesteros, P. Guardabasso, and S. Lizy-Destrez, *Analysis of Lunar Impacts for Orbital Debris Mitigation,* in proceedings of the 73rd International Astronautical Congress (IAC), 2022*,* Paris, France

[2] P. Guardabasso, D. K. Skoulidou, L. Bucci, F. Letizia, S. Lemmens, M. Ansart , X. Roser, S. Lizy-Destrez, G. Casalis, *Analysis of accidental spacecraft break-up events in cislunar space,* vol. 72 (5), pp. 1550-1569, *Advances in Space Research*, 2023, doi: 10.1016/j.asr.2023.05.004

[3] D. C. Davis, K. K. Boudad, S. M. Phillips, and K. C. Howell*, Disposal, deployment, and debris in near rectilinear halo orbits*, in proceedings of the 20th AAS/AIAA Space Flight Mechanics Meeting, 2019, Ka'anapali, Hawaii.

[4] A. Black and C. Frueh, *Fragmentation characterization in the circular restricted three body problem for cislunar space domain awareness,* vol 75 (1), pp. 1177-1204, *Advances in Space Research*, 2025, doi: 10.1016/j.asr.2024.08.076

[5] C. Colombo, E. M. Alessi, W. Van der Weg, S. Soldini, F. Letizia, M. Vetrisano, M. Vasile, A. Rossi, M. Landgraf, *End-of-life disposal concepts for libration point orbit and highly elliptical orbit missions*, vol. 110, pp. 298-312, *Acta Astronautica*, 2015, doi: 10.1016/ j.actaastro.2014.11.002

[6] ESA Space Debris Mitigation Working Group, *Esa space debris mitigation requirements, Tech. rep.*, 2023, available at: https://technology.esa.int/upload/media/ESA-Space-Debris-Mitigation-Requirements-ESSB-ST-U-007-Issue1.pdf. Last accessed: 19-05-2026

[7] V. Szebehely, *Theory of Orbit: The restricted problem of three Bodies*, Academic Press, 1st ed., 1967.

[8] R. Castelli, *On the Relation Between the Bicircular Model and the Coupled Circular Restricted Three-Body Problem Approximation*, In: *Nonlinear and Complex Dynamics* (2011), pp. 53–68, Springer New York

[9] W. S. Koon, M. W. Lo, J. E. Marsden, S. D. Ross, *Dynamical Systems, the Three-Body Problem and Space Mission Design*, Marsden Books, 2011.

[10] E. J. Doedel, V. A. Romanov, R. C. Paffenroth, H. B. Keller, D. J. Dichmann, J. Galán-Vioque, and A. Vanderbauwhede, *Elemental periodic orbits associated with the libration points in the circular restricted 3-body problem*, vol. 17, no. 08, pp. 2625–2677, *International Journal of Bifurcation and Chaos*, 2007, doi: 10.1142/S0218127407018671

[11] Z. P. Olikara, G. Gómez, J. J. Masdemont, *Dynamic mechanisms for spacecraft disposal from Sun-Earth libration points*, vol. 38 (10), pp. 1976–1989, *Journal of Guidance, Control, and Dynamics*, 2015, doi:10.2514/1.G000581

[12] G. Gómez, J. Llibre, R. Martínez, C. Simó, *Station keeping of libration point orbits. ESOC contract 5648/83/D/JS(SC), final report*, European Space Agency, 1985. Reprinted as: *Dynamics and Mission Design Near Libration Points Vol.1 Fundamentals: The Case of Collinear Libration Points*, World Scientific Monograph Series in Mathematics, 2001.